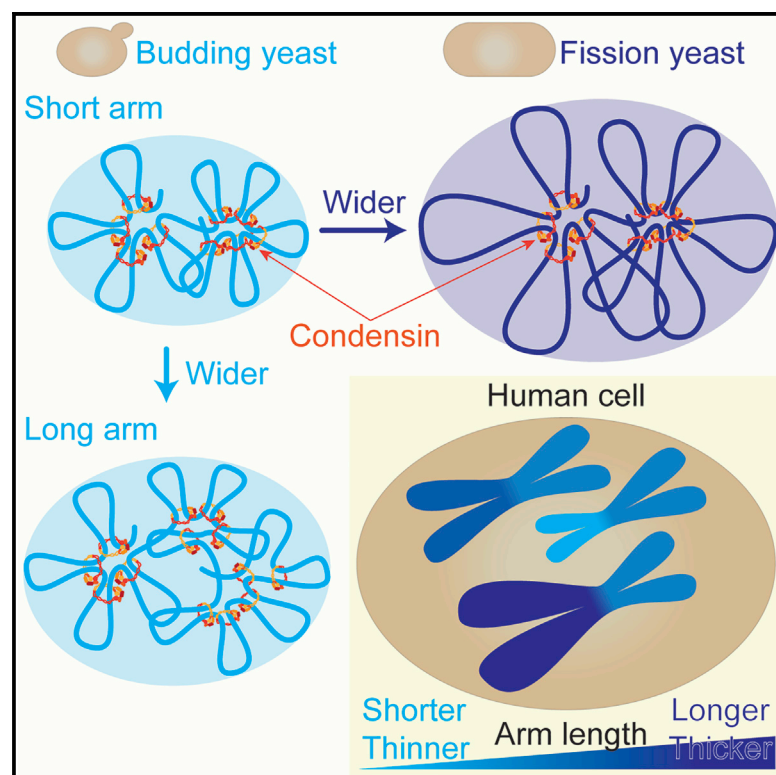# Chromosome arm length, and a species-specific determinant, define chromosome arm width

Graphical abstract

Authors

Yasutaka Kakui, Christopher Barrington, Yoshiharu Kusano, Rahul Thadani, Todd Fallesen, Toru Hirota, Frank Uhlmann

Correspondence

yasukakui@aoni.waseda.jp (Y.K.),
frank.uhlmann@crick.ac.uk (F.U.)

In brief

The factors defining chromosome shape remain an unresolved enigma. Here, Kakui et al. compare chromosome dimensions between yeasts and humans. They find that chromosomes are characterized by species-specific widths but also that within each species, longer chromosome arms are always wider. These observations challenge current models of mitotic chromosome formation.

Highlights

- Chromosomes in fission yeast are thicker than in budding yeast and thinner than in humans

- Chromosome widths correlate with the span of condensin-mediated chromatin contacts

- In each organism, longer chromosome arms are always thicker

- Longer, thicker arms inform mitotic chromosome architecture models

Article

Chromosome arm length, and a species-specific determinant, define chromosome arm width

Yasutaka Kakui,[1,2,3,8,*] Christopher Barrington,[4] Yoshiharu Kusano,[6] Rahul Thadani,[3,7] Todd Fallesen,[5] Toru Hirota,[6] and Frank Uhlmann[3,*]

[1]Waseda Institute for Advanced Study, Waseda University, Tokyo 169-0051, Japan
[2]Laboratory of Cytoskeletal Logistics, Center for Advanced Biomedical Sciences, Waseda University, Tokyo 162-8480, Japan
[3]Chromosome Segregation Laboratory, The Francis Crick Institute, London NW1 1AT, UK
[4]Bioinformatics & Biostatistics Science Technology Platform, The Francis Crick Institute, London NW1 1AT, UK
[5]Advanced Light Microscopy Science Technology Platform, The Francis Crick Institute, London NW1 1AT, UK
[6]Division of Experimental Pathology, Cancer Institute of the Japanese Foundation for Cancer Research, Tokyo 135-8550, Japan
[7]Present address: Department of Biochemistry and Molecular Genetics, University of Colorado Anschutz Medical Campus, Aurora, CO, USA
[8]Lead contact
*Correspondence: yasukakui@aoni.waseda.jp (Y.K.), frank.uhlmann@crick.ac.uk (F.U.)
https://doi.org/10.1016/j.celrep.2022.111753

SUMMARY

Mitotic chromosomes in different organisms adopt various dimensions. What defines these dimensions is scarcely understood. Here, we compare mitotic chromosomes in budding and fission yeasts harboring similarly sized genomes distributed among 16 or 3 chromosomes, respectively. Hi-C analyses and superresolution microscopy reveal that budding yeast chromosomes are characterized by shorter-ranging mitotic chromatin contacts and are thinner compared with the thicker fission yeast chromosomes that contain longer-ranging mitotic contacts. These distinctions persist even after budding yeast chromosomes are fused to form three fission-yeast-length entities, revealing a species-specific organizing principle. Species-specific widths correlate with the known binding site intervals of the chromosomal condensin complex. Unexpectedly, within each species, we find that longer chromosome arms are always thicker and harbor longer-ranging contacts, a trend that we also observe with human chromosomes. Arm length as a chromosome width determinant informs mitotic chromosome formation models.

INTRODUCTION

Mitotic chromosome formation is fundamental to faithful genome inheritance. Each eukaryotic species is characterized by a distinctive number of chromosomes that store its genome.[1] For example, humans harbor 46 chromosomes, as does the Chinese muntjac. The closely related Indian muntjac contains a similarly sized genome within only 7 (male) or 6 (female) chromosomes.[2–4] During cell divisions, the Indian muntjac chromosomes are not only longer but also thicker compared with the Chinese muntjac's shorter and thinner chromosomes. Thicker chromosomes offer a greater degree of DNA compaction, which facilitates segregation of large genome portions within cellular confines. While control over chromosome width is therefore crucial, chromosome width determinants remain poorly understood.

The condensin complex is a key mitotic chromosome constituent.[5,6] Condensin establishes characteristic, mitosis-specific, long-range chromatin contacts that underpin chromosome formation in yeasts and vertebrates.[7–10] Most higher eukaryotes encode two condensin complexes, condensin I and condensin II, whose balance influences mitotic chromosome dimensions.[11–14] How the two condensin complexes discern chromosome length

and width, and how chromosome dimensions are defined in species with a single condensin complex, is not yet known.
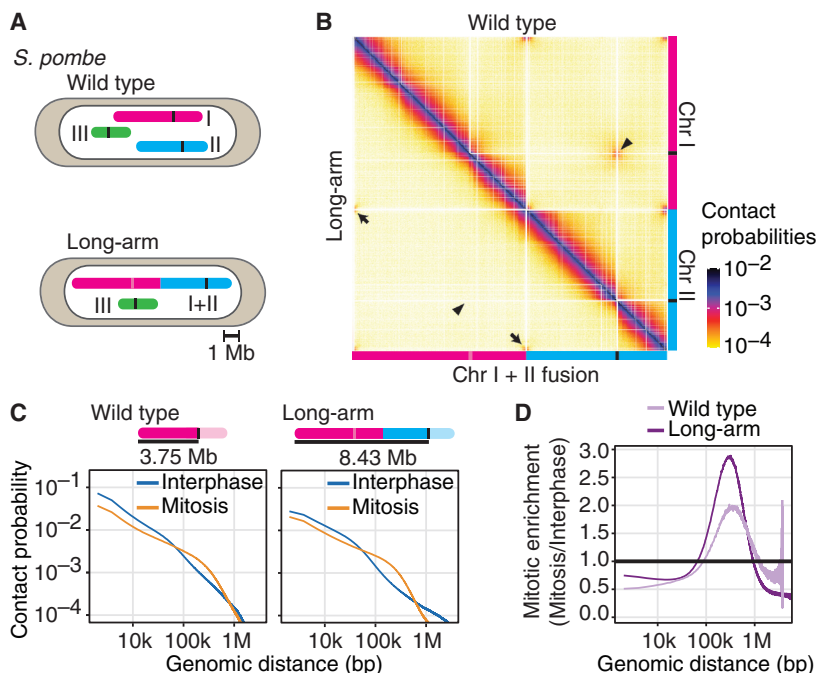
Like the two muntjacs, the budding yeast *Saccharomyces cerevisiae* and the fission yeast *Schizosaccharomyces pombe* harbor genomes of comparable sizes that are distributed, in their case, between 16 and 3 chromosomes.[15,16] While the evolutionary divergence of the two yeast species long predates that of the two muntjacs, chromosomal processes are often conserved through evolution. Here, therefore, we use genetic engineering in the two yeasts to explore chromosome width determinants. We then extend our observations to human chromosomes, revealing that a species-specific determinant, as well as chromosome arm length, shapes chromosome arm width.

RESULTS

Fission-yeast-specific mitotic chromatin contacts

Mitotic chromosomes are characterized by condensin-dependent chromatin contacts in a distance regime that is characteristic for the species under investigation. Mitosis-specific contacts reach from ca. 10 to 100 kb in budding yeast, 90 to 900 kb in fission yeast, and 2 to 20 Mb in human cells.[17] As chromosome lengths in these organisms increase in the same

A

S. pombe
Wild type

Long-arm

1 Mb

B

Wild type

Long-arm

Chr I + II fusion

Chr I

Chr II

Contact probabilities
10^{-2}
10^{-3}
10^{-4}

C

Wild type
3.75 Mb

Long-arm
8.43 Mb

Contact probability
10^{-1}
10^{-2}
10^{-3}
10^{-4}

— Interphase
— Mitosis

10k 100k 1M
Genomic distance (bp)

D

— Wild type
— Long-arm

Mitotic enrichment (Mitosis/Interphase)
3.0
2.5
2.0
1.5
1.0
0.5
0.0

10k 100k 1M
Genomic distance (bp)

Figure 1. Mitosis-specific chromatin contacts in fission yeast
(A) Schematic of chromosome lengths in the *S. pombe* wild-type and long-arm strains. Chromosome II is shown with left and right arms inverted.
(B) Mitotic Hi-C contact maps covering chromosomes I and II in the wild-type (top right) and long-arm (bottom left) strains. Centromere (arrowheads) and telomere (arrows) clustering interactions are highlighted. Data from three biological repeat experiments are compiled. See also Figures S1A and S1B for documentation of the individual repeats experiments and Figure S1C for entire Hi-C contact maps.
(C) Chromatin contact probability as a function of genomic distance along the indicated chromosome arms in the wild-type and long-arm strains.
(D) Mitotic enrichment plot reporting the fold change of chromatin contacts in mitosis relative to interphase. See also Figure S1E for mitotic enrichment plots for all the chromosome arms.

order, we wondered whether the distance regime of mitotic chromatin contacts is determined by chromosome length. To investigate this possibility, we began by comparing a wild-type fission yeast strain with a strain in which chromosomes I and II were fused.[18] The wild-type chromosome I left arm spans 3.75 Mb, while chromosome I fused to the chromosome II right arm results in a total fusion chromosome arm length of 8.43 Mb (Figure 1A, long arm). We performed Hi-C analyses of chromatin interactions in both strains, either growing asynchronously, when most cells reside in G2 phase of the cell cycle, or arrested in mitosis following repression of the anaphase promoting complex activator Slp1.[7] Three biological repeats of the experiments were performed, which produced highly correlated results and were therefore merged for further analyses (Figures S1A and S1B; Table S1).

The Hi-C contact maps confirmed the absence of centromere I in the long-arm strain, which was evident by the lack of centromere clustering interactions that are seen in the wild-type strain (Figures 1B and S1C, arrowheads). Uninterrupted chromatin interactions along the fusion chromosome diagonal further substantiate its continuous nature compared with two distinct chromosome entities seen in the wild-type strain. The fusion point between chromosomes I and II retained detectable interactions with chromosome ends (arrows), suggesting that residual sub-telomeric sequences at the junction are sufficient to engage in telomere clustering.[19]

We now analyzed chromatin interactions that characterize the mitotic state. Chromosome condensation and individualization is manifest as an increased proportion of chromatin contacts within chromosome arms (intra-arm) at the expense of interactions between chromosome arms or between chromosomes.[7,8] This behavior was observed in both the wild-type and long-arm

strains (Figure S1D), suggesting that chromosomes similarly compact and individualize in both strains.

Next, we plotted intra-arm chromatin contact probabilities as a function of genomic distance, comparing the longest respective chromosome arms in the wild-type and long-arm strains. As previously seen,[7,8] the wild-type chromosome I left arm was characterized by increased mitotic interactions in a distance range from 90 to 900 kb. Mitotic chromatin contacts along the fused long arm were enriched in the same distance range (Figure 1C). We then plotted mitotic contact enrichment, i.e., the fold change of the contact probability in mitosis compared with that in interphase, as a function of genomic distance. This confirmed a similar distance range of mitosis-specific interactions along these two arms (Figure 1D), as well as along all other chromosome arms in both the wild-type and long-arm strains (Figure S1E). These observations suggest that fission yeast chromosomes are shaped by similar mitosis-specific chromatin interactions irrespective of their length.

Budding-yeast-specific mitotic chromatin contacts
We next analyzed mitosis-specific chromatin contacts in budding yeast. Chromosome arms in a wild-type strain are around an order of magnitude shorter than in fission yeast (Figure 2A) and are characterized by mitosis-specific interactions that are shorter by a similar factor, in the 10–100 kb range.[9,20] To analyze whether shorter chromosome length is the reason for shorter mitosis-specific interactions, we utilized budding yeast strains in which the 16 chromosomes were merged into 8 or 3 fusion chromosomes.[21] Notably, the 3-chromosome budding yeast strain harbors chromosomes of 2.5–5.6 Mb in length, comparable to the genomic proportions found in fission yeast.

We again used Hi-C to visualize chromatin contacts in these strains, arrested in G1 phase using pheromone a-factor, or in mitosis by nocodazole treatment (Figure S2A). Highly correlated results from three biological repeat experiments were again
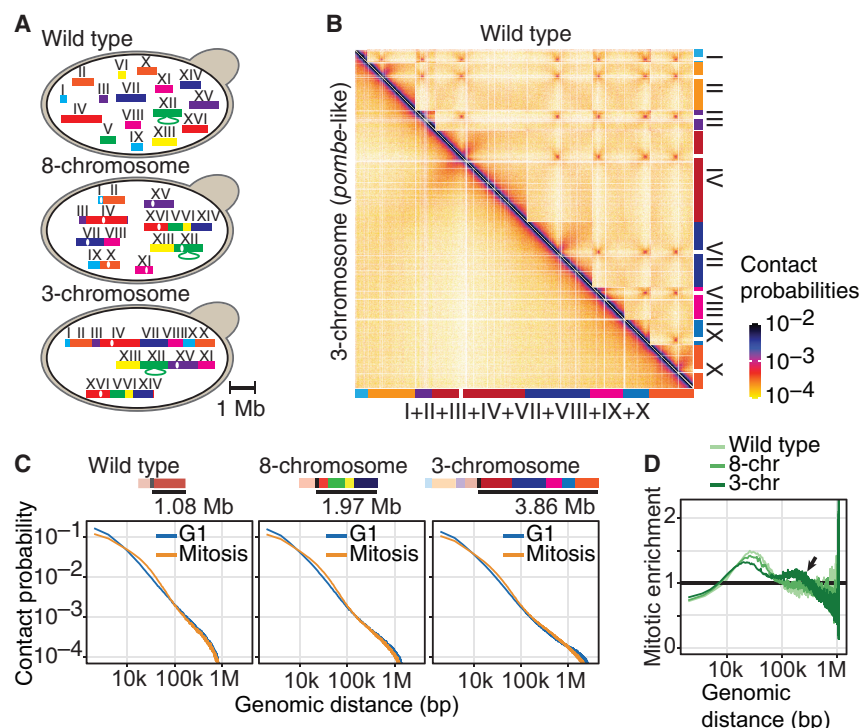
Figure 2. Mitosis-specific chromatin contacts in budding yeast

(A) Schematic of chromosome lengths in the *S. cerevisiae* wild-type, 8-chromosome, and 3-chromosome strains. The rDNA locus on chromosome XII is indicated.

(B) Mitotic Hi-C contact maps covering chromosomes I-IV and VII-X in the wild-type (top right) and 3-chromosome (bottom left) strains. Data from three biological repeat experiments are compiled. See also Figures S2B and S2C for documentation of the individual repeat experiments and Figure S2D for entire Hi-C contact maps in wild-type, 8-chromosome, and 3-chromosome strains.

(C) Chromatin contact probability as a function of genomic distance along the indicated chromosome arms in the wild-type, 8-chromosome, and 3-chromosome strains.

(D) Mitotic enrichment plot along the same chromosome arms. See also Figure S2F for mitotic enrichment plots for all chromosome arms.

merged for analysis (Figures S2B and S2C; Table S1). The mitotic Hi-C maps strikingly confirmed the chromosome fusions, which were seen by absent centromere clustering interactions and formation of the expected numbers of contiguous entities (Figures 2B and S2D).

Mitotic chromosome compaction and individualization were evident in the budding yeast wild type, as well as the 8- and 3-chromosome strains, by the relative increase of intra-chromosome arm interactions (Figure S2E). In the fusion chromosome strains, intra-arm interactions already dominated during interphase. While an increased proportion of intra-arm interactions is a natural consequence of chromosome fusions, we noticed that the fraction of intra-arm interactions was markedly greater in the 3-chromosome budding yeast strain when compared with a wild-type fission yeast strain that also harbors three chromosomes (Figure S1D).

Next, we plotted chromatin contact probabilities as a function of genomic distance along the longest chromosome arm in each of the three strains. As expected, the wild-type chromosome IV long arm was characterized by increased mitotic interactions in the 10–100 kb range. We observed the same for both the 1.97 Mb long arm in the 8-chromosome and the 3.86 Mb long arm in the 3-chromosome strain (Figure 2C). Indeed, mitotic enrichment plots revealed increased interactions in the 10–100 kb range along all chromosome arms in all three strains (Figures 2D and S2F). This reveals that the size range of mitosis-specific chromatin contacts is a budding-yeast-specific chromosome characteristic that is independent of the actual chromosome arm length. This size range is maintained even if chromosomes reach the length of their fission yeast counterparts.

In addition to interactions in the 10–100 kb range, the mitotic enrichment plot of the longest chromosome arm in the 3-chromosome strain revealed another layer of increased interactions, which peaked at around 200 kb (Figure 2D, arrow). To understand the reason for these additional interactions, we used an algorithm that turns the distance constraints contained in Hi-C maps into three-dimensional chromosome representations that best fulfill these constraints (CSynth;[22] Figure S2G). The resulting model of a mitotic 3-chromosome strain revealed higher-order undulation of the chromatin chain, which was not seen in wild-type or 8-chromosome strains. This wave-like pattern, reflecting the 200-kb-range interactions, might have arisen inside nuclei from the spatial constraint imposed on the longest chromosome arm.

A chromosome-arm-length-dependent chromatin interaction pattern

We next compared interaction frequencies along chromosome arms, paying special attention to arm lengths. To do so, we plotted interaction frequencies along each chromosome arm normalized to local (10 kb) chromatin contacts. Local contacts depend on chromatin features that we can assume to be invariant between different chromosome arms (Figure 3A).

On inspection of the resultant interaction frequency plots, we noticed that longer chromosome arms extend their interaction spectrum toward longer-ranging interactions (color-coded in Figure 3A, insets). This arm length-dependent effect was seen in both interphase and mitosis, in both budding yeast and fission yeast. To investigate the origin of longer-ranging contacts along longer chromosome arms, we prepared cumulative interaction plots that depict how interactions at increasing distances make up each chromosome arm's interaction landscape (Figure S3A). These cumulative interaction plots revealed that longer-ranging interactions are not merely the consequence of additional interactions that are possible within longer arms. Rather, shorter
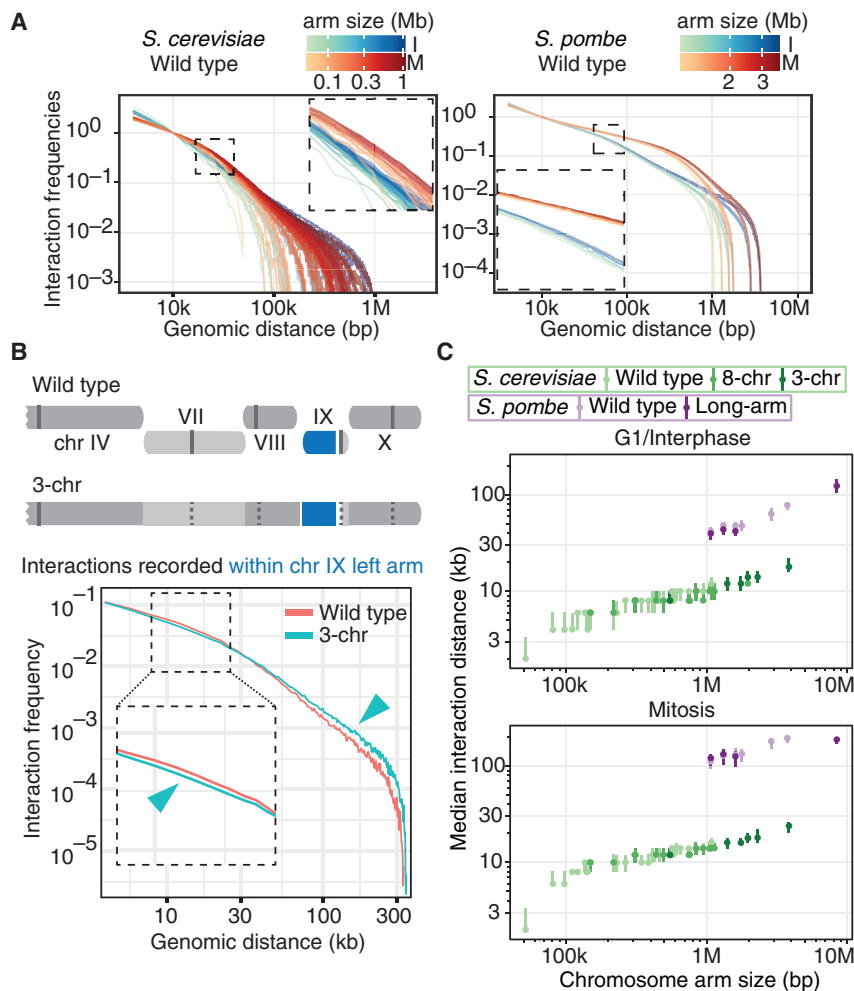
Figure 3. Farther-reaching chromatin contacts within longer chromosomes

(A) Contact probabilities, normalized at 10 kb, within all wild-type budding yeast (left) and fission yeast (right) chromosome arms, color coded for their length, in interphase (I) and mitosis (M).

(B) Comparison of interaction frequencies within the *S. cerevisiae* chromosome IX left arm in the wild-type and 3-chromosome (3-chr) strains. The schematic illustrates interactions recorded within the chromosome IX left arm either as part of wild-type chromosome IX or as part of the chromosome IV-VII-VIII-IX-X fusion. Solid and dotted lines are the positions of centromeres and centromeres removed during chromosome fusion, respectively. Interaction frequencies were recorded exclusively within these identical chromosome IX left arm sequences and plotted. The arrowheads highlight fewer short-range (magnified in the inset) and increased longer-range interactions in the context of the fusion chromosome.

(C) Median interaction distances (25th–75th percentiles indicated) within all *S. cerevisiae* and *S. pombe* chromosome arms in wild-type and chromosome fusions strains in interphase and mitosis. See also Figure S3 for cumulative interaction plots for a comparison of interaction frequencies within all the same arm regions in wild-type and chromosome fusion strains, as well as interaction frequency slope plots.

distance grows with increasing chromosome arm length, both in interphase and in mitosis. This includes wild-type chromosome arms as well as all the fusion chromosome arms. Secondly, we again see a species-specific distinction. Median interaction distances within chromosome arms of the same length are markedly longer in fission yeast when compared with budding yeast.

If typical chromatin interactions span greater distances in longer chromosome arms, then chromatin loop sizes should increase accordingly. The slopes of contact probability plots are often inspected when studying chromatin loop size. Slopes take a negative turn when a typical loop size is reached. Plotting theses contact probability slopes for both budding and fission yeast indeed reveals inflection points at increasing distances as chromosome arm lengths increase (Figure S3C), suggestive of increasing loop sizes. In order to directly compare loop sizes along chromosome arms of increasing lengths, we turned to micro-C data that have described chromatin loops in budding yeast.[23] Indeed, loops with the best loop scores extend to longer distances along longer, when compared with shorter, budding yeast chromosome arms (Figure S3D). Together, these observations reveal that, in addition to species-specific differences, the genomic DNA length of a chromosome arm shapes the intrachromosomal chromatin contact pattern.

Yeast fusion chromosome arms are wider

Longer median interaction distances and larger chromatin loop sizes are indicative of thicker chromosome arms, in which DNA

chromosome arms are characterized by overall shorter-range interactions, while within longer arms, even the most frequent interactions are shifted toward longer distances.
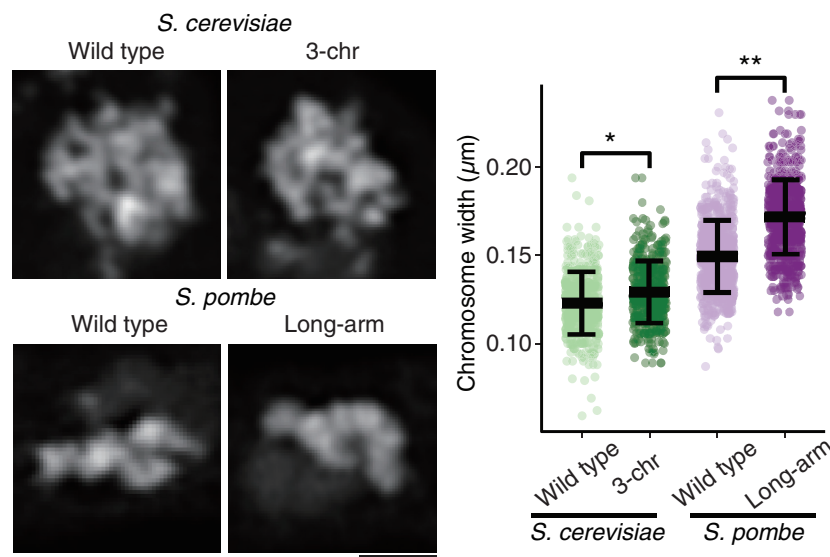
To clarify whether longer-ranging contacts are indeed a chromatin property of longer chromosome arms, rather than simply the consequence of added sequences, we performed the following analysis. We selected, as an example, the budding yeast chromosome IX left arm and plotted contact probabilities exclusively within this chromosome arm region, which were extracted from either the wild type or from the corresponding region of the chromosome fusion strain (Figure 3B). This revealed that the very same sequence segment encompasses fewer short-range interactions and increased longer-ranging interactions when it is part of a longer fusion chromosome. The same was true when comparing each budding or fission yeast chromosome arm within either their wild-type or fusion chromosome contexts (Figure S3B). This confirms that longer chromosome arms are indeed characterized by longer-ranging chromatin contacts.

When we now record the median interaction distance, representing a "typical" interaction span within each chromosome arm (Figure 3C), we make two observations. Firstly, the median interaction

Figure 4. Chromosome widths in budding and fission yeast increase with chromosome length
Examples of DAPI-stained mitotic chromosomes in *S. cerevisiae* wild-type and 3-chr, as well as *S. pombe* wild-type and long-arm, strains. Scale bar, 1 μm. Measured chromosome widths in each strain are shown, and the means and standard deviations indicated. (*p = 1.37 × 10^{-8}, **p = 2.2 × 10^{-16}, Welch's two samples t tests; *S. cerevisiae* wild type, n = 502 from 5 cells; 3-chr, n = 415 from 5 cells; *S. pombe* wild type, n = 527 from 7 cells; long-arm, n = 695 from 6 cells). See also Figure S4 for details and for additional chromosome width measurements.

sequences at greater distances from each other fold back and meet. We therefore explored whether longer chromosome arms are wider. Mitotic budding yeast chromosomes are thought to be too small to be visualized by conventional microscopy. We therefore employed scanning superresolution microscopy (Airyscan[24]) to image mitotic nuclei of wild-type budding yeast cells stained with the DNA dye 4′,6-diamidino-2-phenylindole (DAPI). This revealed discernible linear chromosomes with a mean width of 0.123 ± 0.017 μm (SD) (Figures 4 and S4A). As a complementary superresolution approach, we used structured illumination microscopy,[25] which yielded similar mitotic budding yeast chromosome images visualized by either DAPI staining or fluorescent histone tagging (Htb2-mCitrine; Figure S4B). Chromosome beginnings and ends were hard to ascertain so we were unable to correlate individual chromosome lengths and widths. Instead, we measured chromosome widths in the 3-chromosome strain, in which all chromosomes are longer than their wild-type counterparts. This revealed significantly wider chromosomes measuring 0.129 ± 0.018 μm, consistent with the idea that longer chromosomes are also wider.

To confirm our chromosome width measurements using an additional, unbiased approach, we applied a single Gaussian fit to line traces across chromosomes (Figure S4C). Chromosome widths determined using this semi-automated fitting approach (0.122 ± 0.022 μm for wild type and 0.131 ± 0.012 μm for the 3-chromosome strain in mitosis) were comparable to our manual measurements and support the conclusion that longer fusion chromosome arms are wider. We also applied this measuring approach to budding yeast in G1, when chromosomes appeared distinctly thinner (Figure S4C).

Next, we compared mitotic chromosome widths between the wild-type and long-arm fission yeast strains. The mean chromosome width in the long-arm strain was significantly greater (0.172 ± 0.021 μm) compared with the wild-type strain (0.149 ± 0.020 μm) (Figures 4 and S4D). Again, chromosome

width measurements by Gaussian fitting confirmed increased chromosome widths in the long-arm strain (Figure S4C). This shows that longer fusion chromosome arms are wider in both budding yeast and fission yeast.

When we compare chromosome widths between budding and fission yeast, it is apparent that chromosomes in both the wild-type and long-arm fission yeast strains are substantially wider than those in either the wild-type or 3-chromosome budding yeast strains. Thus, the cytologically determined chromosome widths correlate with chromatin interaction spans measured by Hi-C. A species-specific bracket characterizes budding and fission yeast chromosomes, while, within each species, longer chromosome arms are wider.

Longer human chromosome arms harbor longer-ranging chromatin contacts

Mitotic dimensions can be more accurately measured in higher eukaryotes with larger chromosomes. We therefore investigated chromatin interactions and dimensions of human chromosomes. A Hi-C dataset comparing non-synchronized (mainly interphase) with mitotic human HFF-1 fibroblasts revealed relative mitotic enrichment of chromatin contacts in a 2–20 Mb distance range,[26] which is illustrated in Figure 5A along the chromosome 2 q-arm. Plotting mitotic interaction enrichment next to that of the yeasts illustrates the wider-ranging interactions that act during human mitotic chromosome formation (Figure 5B). Mitosis-specific interactions in the 2–20 Mb regime characterize every human chromosome arm (Figure S5A), suggesting that a common, length-independent principle also underlies human mitotic chromosome formation.

Next, we plotted interaction frequencies normalized to local chromatin contacts (in this case 100 kb) in both interphase and mitosis. This confirmed mitosis-specific interactions in the megabase range and revealed, again, that longer chromosomes always harbor longer-ranging interactions both in interphase and mitosis (Figure S5B). Cumulative interaction plots along each chromosome arm illustrate that typical chromatin interactions reach farther in longer arms (Figure S5C). Displaying the median interaction distances within human chromosome arms next to those in yeasts demonstrates the steady increase of interaction spans, both between the species and as a function of increasing chromosome arm length (Figure 5C).
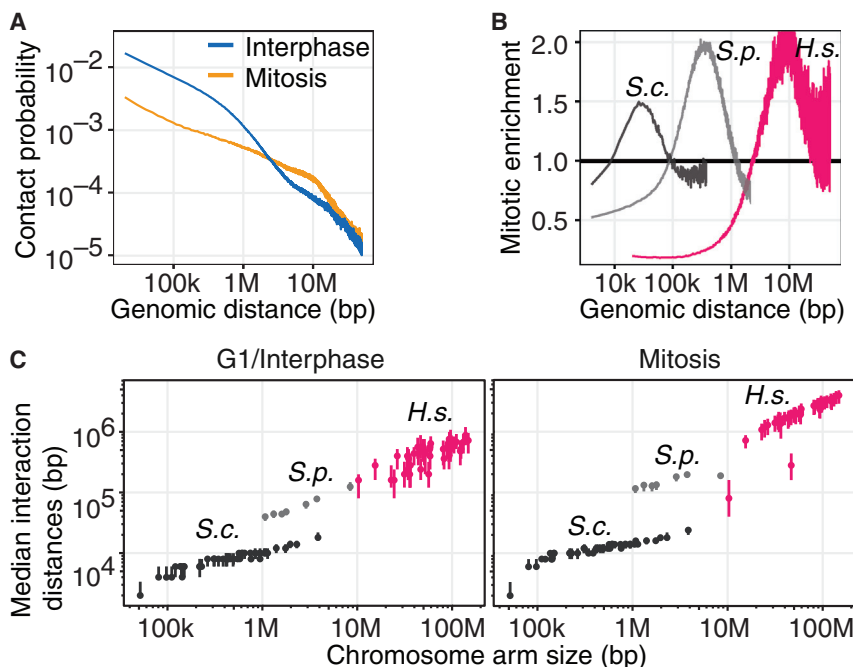
Figure 5. Longer human chromosome arms harbor longer-ranging chromatin contacts

(A) Chromatin contact probability as a function of genomic distance along human chromosome arm 2q in interphase and mitosis. Hi-C data are from Naumova et al.[26]

(B) Mitotic enrichment plot comparing human chromosome arm 2q (*H.s.*) with budding yeast chromosome IV right (*S.c.*) and fission yeast chromosome I left (*S.p.*) arms. See also Figures S5A and S5B for mitotic enrichment and interaction frequency plots of all human chromosome arms.

(C) Median interaction distances (and 25th–75th percentiles) along all human chromosome arms compared with those in budding and fission yeasts. See also Figure S5C for cumulative interaction plots.

Longer human chromosome arms are wider

The above considerations suggest that longer human chromosome arms are wider. To address whether this is the case, we prepared mitotic chromosome spreads from human HeLa cells and measured mitotic chromosome arm lengths and widths following Giemsa staining (Figure 6). Short arms of acrocentric chromosomes were excluded from the analysis to obviate a possible influence from the close-by centromere constriction. These measurements revealed a clear trend in which shorter chromosome arms are thinner while longer chromosome arms are thicker. The correlation between length and width could be approximated by a power-law relationship with an exponent of $\alpha = 0.26$.

A correlation between chromosome arm length and width has, to our knowledge, not been previously reported. We therefore repeated measurements of human chromosome arm dimensions using human diploid retinal pigment epithelial (RPE-1) cells. In this case, to complement the previous approach, we used DAPI staining and fluorescence microscopy for image acquisition. We furthermore developed a semi-automated image analysis tool to obviate any possible measurement bias (Figure S6). The semi-automated quantification of mitotic chromosome arm lengths and widths confirmed a power-law relationship between the two, with the power law exponent derived from the RPE-1 cell measurements somewhat smaller than that observed in HeLa cells. Taken together, our results reveal that longer chromosome arms are wider in both yeasts and human cells.

Condensin shows species-specific spacing but distributes uniformly along short and long chromosome arms

In both yeasts and vertebrates, mitosis-specific chromatin contacts in their respective distance ranges are established by the chromosomal condensin complex. While mitosis-specific interactions are wholly due to condensin in fission yeast and human cells, both condensin and cohesin contribute mitosis-specific contacts in budding yeast.[7–10] How might architecturally similar condensin complexes in these organisms establish mitotic interactions that span such different distances? A feature that likely impacts condensin-dependent chromatin contacts is the spacing of chromosomal condensin-binding sites, i.e., the interval between neighboring condensin-enriched regions. We therefore compared the spacing of condensin binding sites that have been identified in yeast and human cells using chromatin immunoprecipitation.[7,27,28] The median interval between condensin binding sites is 4.1 kb in budding yeast, 11.4 kb in fission yeast, and 107.5 kb along human chromosomes (Figure 7), an increase that parallels increasing mitotic chromatin interaction distances. In the case of budding yeast, the median binding site interval of the cohesin complex[29] is 4.6 kb (Figure S7A), so, in this organism, both condensin and cohesin might contribute chromatin contacts in a similar distance range.

In contrast to clear species-specific differences, condensin binding site intervals among chromosome arms of different lengths were similar in each species (Figure 7). In addition to the condensin peak intervals, we also assessed the total detectable condensin density, inferred from overall chromatin immunoprecipitation (ChIP) sequencing counts, among fission yeast and human chromosome arms. Again, we found no difference in condensin density between shorter and longer chromosome arms (Figure S7B). These observations open the possibility that condensin binding site intervals constitute a molecular determinant that defines the mitotic chromatin interaction range, a chromosomal feature that is species specific but constant among short and long chromosome arms. The possible origin of chromosome-arm-length-dependent chromatin contacts, reaching farther along longer arms in both interphase and in mitosis, will be discussed below.
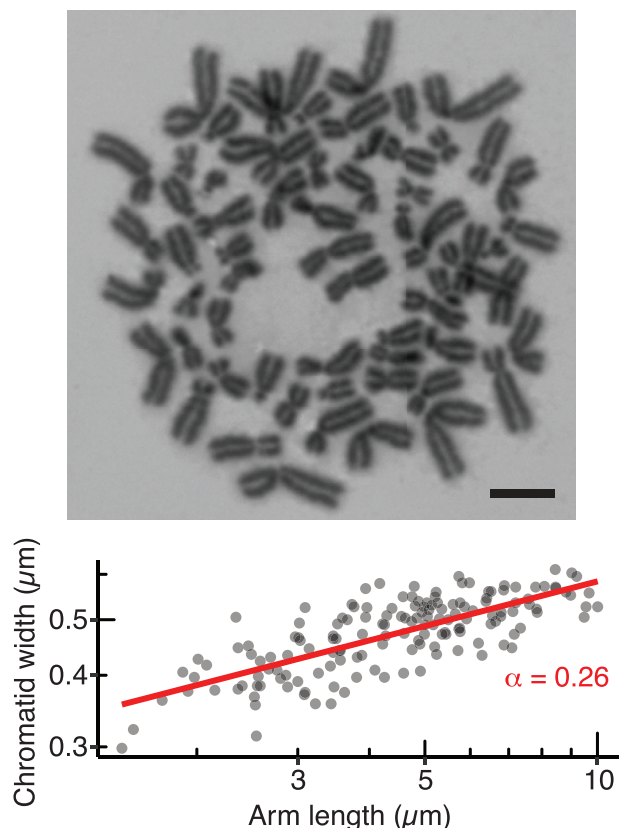
Figure 6. Longer human chromosome arms are wider
Example of a mitotic HeLa cell chromosome spread stained with Giemsa. Scale bar, 5 μm. A correlation plot of manually measured chromosome arm lengths and widths is shown. To avoid possible bias from the centromeric constriction, widths were measured in the middle of each arm. Acrocentric chromosome arms were excluded from the analysis. The red line is a power-law regression line (α = 0.26; n = 157 measurements from 3 cells). See also Figure S6 for semi-automated chromosome arm length and width measurements of DAPI-stained mitotic chromosomes in RPE-1 cells.

DISCUSSION

Our genomic and cytological investigations uncovered and documented two features of mitotic chromosome formation. Firstly, chromosomes are characterized by mitotic contact enrichment in a distance regime that is species specific and independent of a chromosome's genomic length. Secondly, in each species, longer chromosome arms are characterized by farther-reaching chromatin interactions, both in interphase and in mitosis, physically manifest as wider chromosome arms in mitosis.

A species-specific distance regime of mitotic chromatin contacts

Mitosis-specific chromatin contact enrichment occurs in a species-specific distance range, increasing from budding yeast to fission yeast to human. Larger interaction spans correlate with increasing intervals between detectable chromosomal condensin binding sites. Condensin is thought to establish interactions between its binding sites by either diffusion capture or by loop

extrusion.[30–32] In either case, sparser binding sites will connect genomic regions at greater distances from each other. However, median condensin binding site intervals are ∼4, 10, and 100 kb in the three species, while condensin-dependent mitotic contacts reach farther by around an order of magnitude (10–100, 90–900, and 2–20 Mb, respectively). This discrepancy could be explained if not all condensin binding sites, detected by ChIP in a population average, are occupied in individual cells, which would increase the actual spacing between neighboring condensins. Alternatively, more than two condensin binding sites could come together to form condensin foci, as suggested by superresolution images of condensin complexes on fission yeast or human mitotic chromosomes.[30,33] Such condensin foci would bring loci at larger distances into contact. Consistent with the latter possibility, "chromatin interaction analysis by paired-end tag sequencing" (ChIA-PET) has detected condensin-mediated long-range chromatin contacts.[34]

If condensin intervals shape mitotic chromatin contacts, what defines condensin binding sites? In all organisms studied, condensin is found in promoter regions of actively transcribed genes.[27,28,35,36] Genes, in turn, are much longer, and distances between genes greater, in higher eukaryotes with larger genomes. The relationship between gene promoters and condensin-dependent chromatin interactions thus offers an intrinsic mechanism linking genome and chromosome sizes. On the other hand, genes are of comparable length in budding and fission yeasts, yet condensin intervals are larger in fission yeast. Not all active gene promoters recruit condensin,[27,28] and it will be important to further define those chromatin features that turn promoters into condensin binding sites. Depletion of the linker histone H1 from *Xenopus* cell-free extracts led to increased condensin levels and thinner and longer chromosomes.[14] We speculate that intervals between condensin binding sites became shorter in the absence of histone H1, resulting in shorter-range mitotic interactions and, consequently, thinner chromosomes.

In addition to different condensin binding site intervals, the behavior of condensin complexes themselves differ between organisms, e.g., budding yeast condensin turns over faster on chromatin compared with human condensin.[37–39] Therefore, biochemically different behavior could influence chromosome dimensions. Higher eukaryotes typically contain condensin I and condensin II complexes whose relative abundances affect chromosome shape.[11–13,40] The differences between condensin I and condensin II, and how these differences affect chromosome architecture, remain to be explored.

Longer chromosome arms are wider

A surprise came with the realization that, within each species, longer chromosome arms are wider. If, in each species, condensin-mediated mitotic contacts span a constant distance, irrespective of chromosome arm length, then what makes longer arms wider? The solution to this conundrum likely lies with our observation that longer chromosome arms harbor longer-ranging chromatin contacts already in interphase, well before the majority of condensin becomes active. Longer chromosome arms occupy an interphase territory that is not only longer but also wider than that of shorter arms.[41] The addition of diffusion capture interactions between condensin binding sites, acting in
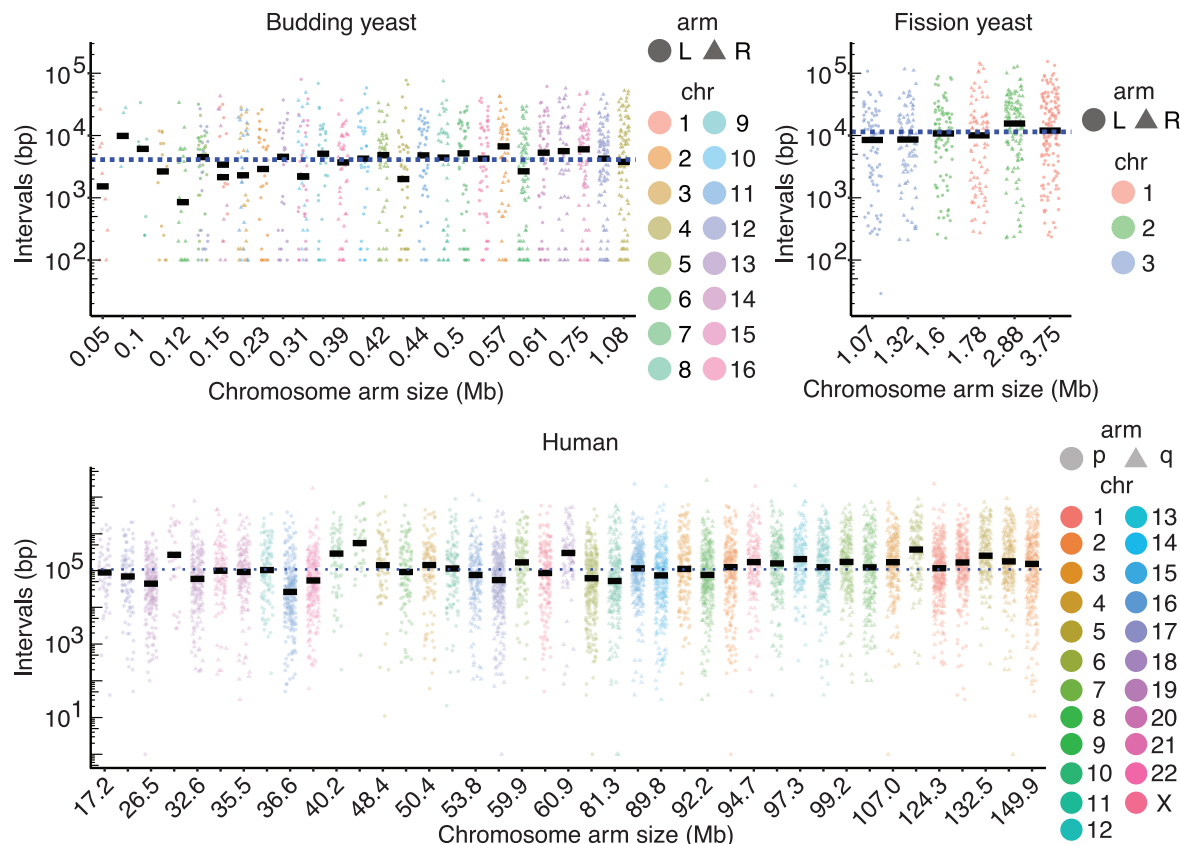
Figure 7. Condensin distribution along yeast and human chromosome arms
Intervals between reported condensin binding sites along budding yeast,[27] fission yeast,[7] and human chromosome arms[28] are displayed. Median intervals along each arm are indicated, and arms are ordered from short to long and identified by their genomic length. The medians of all condensin binding site intervals in each organism are indicated as dotted lines. See also Figure S7 for intervals between budding yeast cohesin binding sites, as well as overall condensin ChIP-sequencing densities, along fission yeast and human chromosomes.

a constant distance range, could then turn interphase territories into mitotic chromosome arms that maintain their interphase aspect ratio. A longer and wider interphase territory will form a longer and wider chromosome arm. We note that, contrary to these observations, the process of loop extrusion predicts that short and long chromosome arms with a similar condensin density develop the same width.[31] Our observations thereby add constraints that inform our thinking about the molecular mechanisms of chromosome formation.

The power-law relationship between arm length and width, which is repeated in the relationship between an arm's genomic length and median interaction distances, is worth further exploration. An exponent of approximately 0.25 means that a 2-fold longer chromosome arm is expected to be around 1.2-fold wider. This relatively small width change suggests that careful measurements will be important when further studying chromosome architecture.

It has, to our knowledge, not been previously reported that longer chromosome arms are wider. Earlier measurements of human prophase chromosome dimensions by scanning electron microscopy have not revealed obvious chromosome width differences when whole chromosomes were considered as a unit

and a chromosome's substantial proteinaceous shell was included in the measurement.[42] A reason for the difference could be our use of Hi-C, as well as DNA stains, specifically to analyze the architecture of a chromosome's DNA compartment. Another reason why a length-width relationship has not previously been noted could be that chromosome arms, insulated at the centromere, form separate units that should be considered independently, i.e., chromosome arm length, not necessarily chromosome length, scales with chromosome arm width. In retrospect, the early pictures of Indian muntjac chromosomes clearly illustrate that longer chromosome arms are also wider.[3] Similarly, microchromosomes in chicken DT40 cells are not only much shorter but also much thinner than their autosome counterparts.[43] In addition to a variety of shapes and sizes in different species, chromosome dimensions change alongside cell-size changes during organismal development and reproduction.[44] Much remains to be learned about the molecular mechanisms that define chromosome dimensions.

Limitations of the study
Our current study is limited to the analysis of two divergent yeast species and human cell lines. We were able to establish an

Cell Reports
Article

accurate physical length-width relationship for human chromosomes but not for yeast chromosomes. The latter were amenable to width, but not to length, determination. Sampling of chromosome dimensions in a wider range of species will be informative, as well as at various stages during development and during mitotic, as well as meiotic, cell divisions. We revealed a striking correlation between the spacing of condensin binding sites and chromosome width. However, it remains to be determined whether this correlation is underpinned by a causal relationship. Future experiments that modulate condensin binding patterns will build on our study and investigate the molecular mechanisms of chromosome formation. These investigations will also consider the contributions of chromosomal proteins additional to condensin and cohesin.

STAR★METHODS

Detailed methods are provided in the online version of this paper and include the following:

- KEY RESOURCES TABLE
- RESOURCE AVAILABILITY
  - Lead contact
  - Materials availability
  - Data and code availability
- EXPERIMENTAL MODEL AND SUBJECT DETAILS
  - Yeast strains
  - Human cell lines
- METHOD DETAILS
  - Yeast chromosome width measurements
  - Semi-automatic human image analysis
  - Hi-C library preparation
  - Hi-C data analysis
  - Micro-C data analysis
  - ChIP data analysis
- QUANTIFICATION AND STATISTICAL ANALYSIS

SUPPLEMENTAL INFORMATION

Supplemental information can be found online at https://doi.org/10.1016/j.celrep.2022.111753.

AUTHOR CONTRIBUTIONS

Y. Kakui and F.U. conceived the study; Y. Kakui performed all yeast experiments; C.B. conducted the bioinformatics analyses; R.T. contributed OMX imaging; Y. Kusano and T.H. performed human cell experiments; T.F. provided image analysis tools; and Y. Kakui and F.U. wrote the manuscript with input from all coauthors.

DECLARATION OF INTERESTS

The authors declare no competing interests.

REFERENCES

1. Sumner, A.T. (2003). Chromosomes - Organization and Function (Blackwell Publishing).

2. Wurster, D.H., and Benirschke, K. (1967). Chromosome studies in some deer, the springbok, and the pronghorn, with notes on placentation in deer. Cytologia *32*, 273–285.

3. Wurster, D.H., and Benirschke, K. (1970). Indian muntjac, Muntiacus muntjak: a deer with a low diploid chromosome number. Science *168*, 1364–1366.

4. Mudd, A.B., Bredeson, J.V., Baum, R., Hockemeyer, D., and Rokhsar, D.S. (2020). Analysis of muntjac deer genome and chromatin architecture reveals rapid karyotype evolution. Commun. Biol. *3*, 480.

5. Hirano, T. (2016). Condensin-based chromosome organization from bacteria to vertebrates. Cell *164*, 847–857.

6. Uhlmann, F. (2016). SMC complexes, from DNA to chromosomes. Nat. Rev. Mol. Cell Biol. *17*, 399–412.

7. Kakui, Y., Rabinowitz, A., Barry, D.J., and Uhlmann, F. (2017). Condensin-mediated remodeling of the mitotic chromatin landscape in fission yeast. Nat. Genet. *49*, 1553–1557.

8. Tanizawa, H., Kim, K.-D., Iwasaki, O., and Noma, K.I. (2017). Architectural alterations of the fission yeast genome during the cell cycle. Nat. Struct. Mol. Biol. *24*, 965–976.

9. Schalbetter, S.A., Goloborodko, A., Fudenberg, G., Belton, J.-M., Miles, C., Yu, M., Dekker, J., Mirny, L., and Baxter, J. (2017). SMC complexes differentially compact mitotic chromosomes according to genomic context. Nat. Cell Biol. *19*, 1071–1080.

10. Gibcus, J.H., Samejima, K., Goloborodko, A., Samejima, I., Naumova, N., Nuebler, J., Kanemaki, M.T., Xie, L., Paulson, J.R., Earnshaw, W.C., et al. (2018). A pathway for mitotic chromosome formation. Science *359*. eaao6135.

11. Ono, T., Losada, A., Hirano, M., Myers, M.P., Neuwald, A.F., and Hirano, T. (2003). Differential contributions of condensin I and condensin II to mitotic chromosome architecture in vertebrate cells. Cell *115*, 109–121.

12. Shintomi, K., and Hirano, T. (2011). The relative ratio of condensin I to II determines chromosome shapes. Genes Dev. *25*, 1464–1469.

13. Green, L.C., Kalitsis, P., Chang, T.M., Cipetic, M., Kim, J.H., Marshall, O., Turnbull, L., Whitchurch, C.B., Vagnarelli, P., Samejima, K., et al. (2012). Contrasting roles of condensin I and condensin II in mitotic chromosome formation. J. Cell Sci. *125*, 1591–1604.

14. Choppakatla, P., Dekker, B., Cutts, E.E., Vannini, A., Dekker, J., and Funabiki, H. (2021). Linker histone H1.8 inhibits chromatin binding of condensins and DNA topoisomerase II to tune chromosome length and individualization. Elife *10*. e68918.

15. Goffeau, A., Aert, R., Agostini-Carbone, M.L., Ahmed, A., Aigle, M., Alberghina, L., Albermann, K., Albers, M., Aldea, M., Alexandraki, D., et al. (1997). The yeast genome directory. Nature *387*, 5.

16. Wood, V., Gwilliam, R., Rajandream, M.-A., Lyne, M., Lyne, R., Stewart, A., Sgouros, J., Peat, N., Hayles, J., Baker, S., et al. (2002). The genome sequence of *Schizosaccharomyces pombe*. Nature *415*, 871–880.

17. Kakui, Y., and Uhlmann, F. (2018). SMC complexes orchestrate the mitotic chromatin interaction landscape. Curr. Genet. *64*, 335–339.

18. Ohno, Y., Ogiyama, Y., Kubota, Y., Kubo, T., and Ishii, K. (2016). Acentric chromosome ends are prone to fusion with functional chromosome ends

through a homology-directed rearrangement. Nucleic Acids Res. *44*, 232–244.

19. Matsuda, A., Chikashige, Y., Ding, D.-Q., Ohtsuki, C., Mori, C., Asakawa, H., Kimura, H., Haraguchi, T., and Hiraoka, Y. (2015). Highly condensed chromatins are formed adjacentto subtelomeric and decondensed silent chromatinin fission yeast. Nat. Commun. *6*, 7753.

20. Lazar-Stefanita, L., Scolari, V.F., Mercy, G., Muller, H., Guérin, T.M., Thierry, A., Mozziconacci, J., and Koszul, R. (2017). Cohesin and condensins orchestrate the 4D dynamics of yeast chromosomes during the cell cycle. EMBO J. *36*, 2684–2697.

21. Shao, Y., Lu, N., Wu, Z., Cai, C., Wang, S., Zhang, L.-L., Zhou, F., Xiao, S., Liu, L., Zeng, X., et al. (2018). Creating a functional single-chromosome yeast. Nature *560*, 331–335.

22. Todd, S., Todd, P., McGowan, S.J., Hughes, J.R., Kakui, Y., Leymarie, F.F., Latham, W., and Taylor, S. (2021). CSynth: an interactive modelling and visualization tool for 3D chromatin structure. Bioinformatics *37*, 951–955.

23. Costantino, L., Hsieh, T.-H.S., Lamothe, R., Darzacq, X., and Koshland, D. (2020). Cohesin residency determines chromatin loop patterns. Elife *9*, e59889.

24. Huff, J. (2015). The Airyscan detector from ZEISS: confocal imaging with improved signal-to-noise ratio and super-resolution. Nat. Methods *12*, 111–130.

25. Dobbie, I.M., King, E., Parton, R.M., Carlton, P.M., Sedat, J.W., Swedlow, J.R., and Davis, I. (2011). OMX: a new platform for multi-modal, multi-channel widefield imaging. Cold Spring Harb. Protoc. *2011*, 899–909.

26. Naumova, N., Imakaev, M., Fudenberg, G., Zhan, Y., Lajoie, B.R., Mirny, L.A., and Dekker, J. (2013). Organization of the mitotic chromosome. Science *342*, 948–953.

27. D'Ambrosio, C., Schmidt, C.K., Katou, Y., Kelly, G., Itoh, T., Shirahige, K., and Uhlmann, F. (2008). Identification of *cis*-acting sites for condensin loading onto budding yeast chromosomes. Genes Dev. *22*, 2215–2227.

28. Sutani, T., Sakata, T., Nakato, R., Masuda, K., Ishibashi, M., Yamashita, D., Suzuki, Y., Hirano, T., Bando, M., and Shirahige, K. (2015). Condensin targets and reduces unwound DNA structures associated with transcription in mitotic chromosome condensation. Nat. Commun. *6*, 7815.

29. Muñoz, S., Minamino, M., Casas-Delucchi, C.S., Patel, H., and Uhlmann, F. (2019). A role for chromatin remodeling in cohesin loading onto chromosomes. Mol. Cell *74*, 664–673.e5.

30. Gerguri, T., Fu, X., Kakui, Y., Khatri, B.S., Barrington, C., Bates, P.A., and Uhlmann, F. (2021). Comparison of loop extrusion and diffusion capture as mitotic chromosome formation pathways in fission yeast. Nucleic Acids Res. *49*, 1294–1312.

31. Goloborodko, A., Imakaev, M.V., Marko, J.F., and Mirny, L. (2016). Compaction and segregation of sister chromatids via active loop extrusion. Elife *5*, e14864.

32. Cheng, T.M.K., Heeger, S., Chaleil, R.A.G., Matthews, N., Stewart, A., Wright, J., Lim, C., Bates, P.A., and Uhlmann, F. (2015). A simple biophysical model emulates budding yeast chromosome condensation. Elife *4*, e05565.

33. Walther, N., Hossain, M.J., Politi, A.Z., Koch, B., Kueblbeck, M., Ødegård-Fougner, Ø., Lampe, M., and Ellenberg, J. (2018). A quantitative map of human Condensins provides new insights into mitotic chromosome architecture. J. Cell Biol. *217*, 2309–2328.

34. Kim, K.-D., Tanizawa, H., Iwasaki, O., and Noma, K.I. (2016). Transcription factors mediate condensin recruitment and global chromosomal organization in fission yeast. Nat. Genet. *48*, 1242–1252.

35. Kranz, A.-L., Jiao, C.-Y., Winterkorn, L.H., Albritton, S.E., Kramer, M., and Ercan, S. (2013). Genome-wide analysis of condensin binding in *Caenorhabditis elegans*. Genome Biol. *14*, R112.

36. Nakazawa, N., Sajiki, K., Xu, X., Villar-Briones, A., Arakawa, O., and Yanagida, M. (2015). RNA pol II transcript abundance controls condensin accumulation at mitotically up-regulated and heat-shock-inducible genes in fission yeast. Gene Cell. *20*, 481–499.

37. Gerlich, D., Hirota, T., Koch, B., Peters, J.-M., and Ellenberg, J. (2006). Condensin I stabilizes chromosomes mechanically through a dynamic interaction in live cells. Curr. Biol. *16*, 333–344.

38. Thadani, R., Kamenz, J., Heeger, S., Muñoz, S., and Uhlmann, F. (2018). Cell-cycle regulation of dynamic chromosome association of the condensin complex. Cell Rep. *23*, 2308–2317.

39. Robellet, X., Thattikota, Y., Wang, F., Wee, T.-L., Pascariu, M., Shankar, S., Bonneil, É., Brown, C.M., and D'Amours, D. (2015). A high-sensitivity phospho-switch triggered by Cdk1 governs chromosome morphogenesis during cell division. Genes Dev. *29*, 426–439.

40. Thadani, R., Uhlmann, F., and Heeger, S. (2012). Condensin, chromatin crossbarring and chromosome condensation. Curr. Biol. *22*, R1012–R1021.

41. Dietzel, S., Jauch, A., Kienle, D., Qu, G., Holtgreve-Grez, H., Eils, R., Münkel, C., Bittner, M., Meltzer, P.S., Trent, J.M., and Cremer, T. (1998). Separate and variably shaped chromosome arm domains are disclosed by chromosome arm painting in human cell nuclei. Chromosome Res. *6*, 25–33.

42. Booth, D.G., Beckett, A.J., Molina, O., Samejima, I., Masumoto, H., Kouprina, N., Larionov, V., Prior, I.A., and Earnshaw, W.C. (2016). 3D-CLEM reveals that a major portion of mitotic chromosomes is not chromatin. Mol. Cell *64*, 790–802.

43. Hudson, D.F., Vagnarelli, P., Gassmann, R., and Earnshaw, W.C. (2003). Condensin is required for nonhistone protein assembly and structural integrity of vertebrate mitotic chromosomes. Dev. Cell *5*, 323–336.

44. Hara, Y., Iwabuchi, M., Ohsumi, K., and Kimura, A. (2013). Intranuclear DNA density affects chromosome condensation in metazoans. Mol. Biol. Cell *24*, 2442–2453.

45. O'Reilly, N., Charbin, A., Lopez-Serra, L., and Uhlmann, F. (2012). Facile synthesis of budding yeast **a**-factor and its use to synchronize cells of a mating type. Yeast *29*, 233–240.

46. Li, H. (2013). Aligning sequence reads, clone sequences and assembly contigs with BWA-MEM. Preprint at arXiv. https://doi.org/10.48550/arXiv.1303.3997.

47. Matthey-Doret, C., Baudry, L., Breuer, A., Montagne, R., Guiglielmoni, N., Scolari, V., Jean, E., Campeas, A., Chanut, P.H., Oriol, E., et al. (2020). Computer vision for pattern detection in chromosome contact maps. Nat. Commun. *11*, 5795.

48. Kakui, Y., Barrington, C., Barry, D.J., Gerguri, T., Fu, X., Bates, P.A., Khatri, B.S., and Uhlmann, F. (2020). Fission yeast condensin contributes to interphase chromatin organization and prevents transcription-coupled DNA damage. Genome Biol. *21*, 272.

STAR★METHODS

KEY RESOURCES TABLE

REAGENT or RESOURCE	SOURCE	IDENTIFIER
Chemicals, peptides, and recombinant proteins		
a-factor	O'Reilly et al. 2012[45]	N/A
Nocodazole	Sigma-Aldrich	M1404
DAPI	Sigma-Aldrich	D9542
cOmplete ULTRA tablets Mini EDTA-free	Sigma-Aldrich	5892791001
RO-3306	Enzo Life Science	ALX-270-463-M005
ProLong Gold antifade	MOP	P36930
Entellan embedding agent	Merck	1.07961.0100
Giemsa's azur-eosin-methylene blue solution	Merk	1.09204.0503
Gurr buffer tablet	GIBCO	10582-013
PhosSTOP	Sigma-Aldrich	4906837001
DpnII (5000 U)	NEB	R0543M
T4 DNA ligase (100,000 U)	NEB	M0202L
Biotin-dATP	Thermo Fisher Scientific	19524016
dATP (10 mM)	Thermo Fisher Scientific	18252015
dGTP (10 mM)	Thermo Fisher Scientific	18254011
dTTP (10 mM)	Thermo Fisher Scientific	18255018
dCTP (10 mM)	Thermo Fisher Scientific	18253013
Klenow (1000U)	NEB	M0210L
Proteinase K	Thermo Fisher Scientific	EO0492
Phenol:Chloroform:Isoamyl Alc 25:24:1	Sigma	P2069-100ML
Phase lock tube Heavy	Quantabio	2302830
ClonAmp 2x Premix	Clontech	639298
T4 DNA polymerase (3000 U)	NEB	M0203L
SPRI select beads	BECKMAN COULTER	B23317
NEBNext Ultra II kit	NEB	E7645S
Dynabeads MyOne Streptavidin C1	invitrogen	DB65001
NEBNext Ultra II Q5 2x PCR Master Mix	NEB	M0544L
NEBNext Multiplex Oligos for Illumina (Index Primers Set1)	NEB	E7335S
Deposited data		
S. cerevisiae Brn1 ChIP	D'Ambrosio et al. 2008[27]	GEO: GSE12149
S. cerevisiae micro-C data	Costantino et al., 2020[23]	GEO: GSE151553
S. pombe Cnd2 ChIP	Kakui et al., 2017[7]	GEO: GSE94478
S. pombe wild type Hi-C data	Kakui et al., 2017[7]	GEO: GSE94478
Human HFF-1 cell Hi-C data	Naumova et al., 2013[26]	https://www.ebi.ac.uk/arrayexpress/experiments/E-MTAB-1948/
HeLa CAP-G ChIP	Sutani et al., 2015[28]	GEO: SRP045410
Raw and processed data	This paper	GEO: GSE148307
Experimental models: Cell lines		
Human: HeLa	S. Narumiya, Kyoto University	N/A
Human: hTERT-RPE-1	ATCC Cell Bank	Cat# CRL-4000; RRID: CVCL_4388

(Continued on next page)

Continued

REAGENT or RESOURCE	SOURCE	IDENTIFIER
Experimental models: Organisms/strains		
A list of yeast strains used in this study can be found in Table S2.	N/A	N/A
Software and algorithms		
Distiller v0.3.3	N/A	github.com/open2c/distiller-nf
bwa v0.17.7	Li, 2013[46]	N/A
cooler v0.8.5	N/A	github.com/open2c/cooler
rhdf5 library v2.24.0	N/A	github.com/grimbough/rhdf5
liftOver v369	N/A	http://hgdownload.soe.ucsc.edu/admin/exe/
Chromosight v1.6.2	Matthey-Doret et al., 2020[47]	N/A
nf-core/chipseq	N/A	https://doi.org/10.1038/s41587-020-0439-x
ImageJ/Fiji	Open-source	http://fiji.sc
Rstudio	Rstudio, PBC	http://www.rstudio.com/
MATLAB	MathWorks	https://matlab.mathworks.com
MATLAB script of the image analysis tool for semi-automated chromosome width measurements.	This paper	https://doi.org/10.6084/m9.figshare.19383587
Other		
Raw and processed data relating to the semi-automatic human chromosome width measurements.	This paper	https://doi.org/10.6084/m9.figshare.19383587

RESOURCE AVAILABILITY

Lead contact
Further information and requests for resources and reagents should be directed to and will be fulfilled by the lead contact, Yasutaka Kakui (yasukakui@aoni.waseda.jp).

Materials availability
Unique reagents generated in this study are available upon reasonable request from the lead contact without restrictions.

Data and code availability
- The Hi-C datasets generated in this study are available at the Gene Expression Omnibus with identifier GSE148307.
- The original code (MATLAB script) of the image analysis tool developed in this study, as well as the full image data, are available from figshare at https://doi.org/10.6084/m9.figshare.19383587.
- Any additional information required to reanalyze the data reported in this paper is available from the lead contact upon request.

EXPERIMENTAL MODEL AND SUBJECT DETAILS

Yeast strains
Yeast strains used in this study are listed in Table S2. Budding yeast was grown in YP medium containing 2% glucose (YPD) at 25°C. *MATα* cells were arrested in G1 by adding 0.02 μg/mL a-factor[45] every hour for 2.5 h. *MAT*a cells were arrested in the same way using 0.4 μg/mL α-factor. For block in mitosis, G1-arrested cells were filtered, washed, and released into YPD containing 15 μg/mL of nocodazole and grown for 90 min. Fission yeast was cultured in YE medium containing 2% glucose and adenine, leucine, uracil, histidine and lysine supplements (YE5S) at 25°C. Mitotic arrest by Slp1 shut-off under control of the thiamine-repressible *nmt41* promoter was achieved by growth in minimal medium with 2% glucose, 3.75 mg/mL of glutamate and the 5 supplements (PMG5S), followed by transfer into YE5S for 4 h.

Human cell lines
RPE-1 and HeLa cells were maintained in DMEM supplemented with 10% fetal calf serum, 0.2 mM L-glutamine, 100 U/mL penicillin and 100 μg/mL streptomycin at 37°C in a 5% CO_2 environment. Mitotic cells were collected by shake off, 30 min after release from 3 h G2/M synchronization by 9 μM RO-3306 treatment. After 5 min incubation with hypotonic buffer (PBS:H_2O = 3:7), cells were fixed with

fresh Carnoy's solution (70% methanol, 30% acetic acid). To prepare chromosome spreads, fixed cells were dried on glass slides, followed by either 5 μg/mL DAPI or Giemsa staining, then mounted in ProLong Gold antifade (Invitrogen) or Entellan embedding agent (Merck), respectively. HeLa chromosome images were acquired with a Zeiss microscope, 64x objective lens and a PRIME BSI camera, RPE-1 cell images with a LSM880 microscope and 63x objective lens in airyscan mode. Lengths and widths at mid-length of all clearly identifiable Giemsa-stained HeLa chromosome arms were measured using the line tool in ImageJ. Acrocentric arms were excluded from the analysis.

METHOD DETAILS

Yeast chromosome width measurements

Cells were fixed in 70% ethanol and stained with DAPI, or imaged without staining when visualizing histone-fluorescent protein fusions. Images were acquired along the z axis in 0.15 μm intervals using an Airyscan 2 LSM980 microscope (Zeiss) equipped with a 63x/1.40 NA objective lens. Chromosome widths in single focal planes were measured using the line tool in Fiji. To reduce selection bias, we measured arm widths in all focal planes and at all places where individual chromosome arms were accessible (at least 39, but typically between 100 and 168 measurements per nucleus). To determine chromosome widths by Gaussian fitting, line profiles across yeast chromosomes in single focal planes were obtained in Fiji. The best Gaussian fits for chromosome intensities were determined using Curve in MATLAB. Chromosome width was then defined as the Gaussian width at half maximum.

Semi-automatic human image analysis

Z-stacks of DAPI-stained RPE-1 chromosome spreads were acquired, and maximum intensity projected. All straight, non-overlapping chromosome arms were cropped as individual images. A MATLAB script was now utilized (available at https://doi.org/10.6084/m9.figshare.19383587) that performed the following steps. A double Gaussian fit to capture both sister arms was applied at every pixel row along the arm length. The width at half maximum intensity was calculated from the fit. To avoid the centromere constriction, arm positions with less than 70% of the average width were removed. The arm length was then defined as the distance between the 70% width boundaries. The arm width is the mean of the widths from all included pixel rows. Widths of sister arms were calculated independently.

Hi-C library preparation

Fission and budding yeast cells were fixed at 25°C for 30 min with 0.5% and 1% formaldehyde, respectively. Hi-C libraries were prepared and sequenced as described.[48] The human Hi-C data was from Naumova et al.[26]

Hi-C data analysis

S. pombe (ASM294v2) and *S. cerevisiae* (BY4742) genomes were rearranged using SnapGene to create in silico-fused chromosomes as required. The sequence and coordinates were readout in both FastA and Bed formats.

Distiller v0.3.3 (github.com/open2c/distiller-nf) was used to align reads, filter alignments and aggregate and balance interaction matrices. Technical replicates of sequenced libraries were aligned to the respective genomes using bwa v0.17.7[46] and merged with biological replicates from which PCR duplicates were removed. Low-confidence (mapq<30) and very near *cis* alignments (<1kb) were removed. Interaction matrices were generated at a base resolution of 500 bp and aggregated into matrices of 1, 2, 5, 7.5, 10- 15, 20 and 50 kb and balanced using ICE. Balanced matrices were saved in.cool and.mcool formats.

Interaction matrices were queried using the cooler v0.8.5 dump function (github.com/open2c/cooler) or the rhdf5 library v2.24.0 (github.com/grimbough/rhdf5). Interaction frequency profiles as a function of genomic distance were calculated using 2 kb binned interaction matrices (10 kb for the human datasets) and defined as the sum of contacts at each genomic separation as a proportion of the total contacts.

To display the first derivative (slope), a spline was fitted to the profile using the sm.spline function of the pspline R package. The slope of the smoothed profile was then calculated using the predict R function.

Median interaction distances were calculated using 2 kb resolution interaction matrices (40 kb for human datasets) across arms, with a 20 kb exclusion at either end (200 kb for human datasets). For each bin, its median contact distance amongst all interactions was determined. For each arm, the median of those 'bin' medians was determined as 'median interaction distance'.

Cumulative intra-arm interaction profiles were calculated at 2 kb resolution (1 Mb for human). For each bin, interaction scores were collected from the.cool file and the total score at all distances from the bin calculated. A cumulative profile of interaction scores along ranked absolute distance between bins was then calculated and scaled to the sum of all contacts.

To compare interaction frequency distribution within the same chromosome arm regions between wild type and chromosome fusions strains, a liftOver chain was created to translate genomic coordinates between genomic contexts (using the liftOver package downloaded from http://hgdownload.soe.ucsc.edu/admin/exe/). Using liftOver and the liftOver chain we then determine the position of a wild type chromosome arm in the fusion genome to directly compare the same genomic region in either genomic context.

Micro-C data analysis

S. cerevisiae micro-C data A364 from GSE151553 were[23] prepared into.cool and.mcool files, as above, using distiller. The 1 kb resolution merged-replicate matrix was then analyzed by Chromosight version 1.6.2[47] to identify loops using pattern = loops,

perc_undetected = 0.2, min-dist = 5000 and max-dist = 100000 with all other parameters left as default. The identified loops were additionally filtered to remove loops on chromosome arms with fewer than 15 detected loops. This filter removed 84 of 1,080 loops on 8 chromosome arms. Loop scores calculated by Chromosight detect were then plotted against loop size and a smoothed line fitted through the data using the geom_smooth function of ggplot2. Loop size with the maximum smoothed loop score on each chromosome arm was then plotted as a function of chromosome arm length.

ChIP data analysis

The ChIP peak interval analysis used published condensin peak lists for *S. cerevisiae*,[27] *S. pombe* (GSE94478) and HeLa cells (SRP045410). The *S. cerevisiae* cohesin peak list was derived from.[29] To assess overall condensin binding, ChIP-Seq data were re-analyzed using the nf-core/chipseq pipeline (https://doi.org/10.1038/s41587-020-0439-x). The first 23 kb and last 145 kb on *S. pombe* chromosome III, next to the rDNA repeats, were excluded. Human chr13p, chr14p, chr15p, chr21p, chr22p, chrYp and chrYq showed <10% input read density compared to any other arm, possibly due to mapping ambiguities, and were therefore excluded. The read numbers in the ChIP datasets were normalized using the input read numbers.

QUANTIFICATION AND STATISTICAL ANALYSIS

Chromosome width quantifications were performed manually in yeast and HeLa cells, or using semi-automated image analyses, as described in more detail in the method details. Statistical analyses were performed using the t.test function in R.